nature neuroscience

Olfactory behavior and physiology are disrupted in prion protein knockout mice

Claire E Le Pichon[1], Matthew T Valley[1], Magdalini Polymenidou[2,3], Alexander T Chesler[1], Botir T Sagdullaev[1,3], Adriano Aguzzi[2] & Stuart Firestein[1]

The prion protein PrP^C is infamous for its role in disease, but its normal physiological function remains unknown. Here we found a previously unknown behavioral phenotype of *Prnp*$^{-/-}$ mice in an odor-guided task. This phenotype was manifest in three *Prnp* knockout lines on different genetic backgrounds, which provides strong evidence that the phenotype is caused by a lack of PrP^C rather than by other genetic factors. *Prnp*$^{-/-}$ mice also showed altered behavior in a second olfactory task, suggesting that the phenotype is olfactory specific. Furthermore, PrP^C deficiency affected oscillatory activity in the deep layers of the main olfactory bulb, as well as dendrodendritic synaptic transmission between olfactory bulb granule and mitral cells. Notably, both the behavioral and electrophysiological alterations found in *Prnp*$^{-/-}$ mice were rescued by transgenic neuronal-specific expression of PrP^C. These data suggest that PrP^C is important in the normal processing of sensory information by the olfactory system.

Despite two decades of research, the function of the cellular prion protein PrP^C is still unknown. It had been hoped the *Prnp*$^{-/-}$ mouse would provide evidence for the function of this protein that is so widely expressed in all vertebrates, at all stages and in almost all tissues, especially in the brain. Such ubiquity suggests that PrP^C might perform some essential cellular function. However, the first *Prnp*$^{-/-}$ mouse showed no overt phenotype, implying that the protein was dispensable[1]. Instead, the major finding in *Prnp*$^{-/-}$ mice was their resistance to prion disease[2].

Nevertheless, it is unlikely that the PrP protein would have evolved simply to enable a rare fatal disease. Indeed, since the initial knockout mouse study, a host of subtle phenotypes have been described, ranging from behavioral changes to electrophysiological and biochemical alterations[3]. The reported behavioral phenotypes are of a disparate nature, as might be expected from the widespread expression pattern of PrP^C in the brain. They include altered circadian rhythm[4], modified sleep patterns[5], impaired spatial learning behavior in the Barnes circular maze[6] and increased sensitivity to seizure[7,8].

Despite the wide gamut of behaviors that have been tested in PrP knockouts, almost all have relied on spatiovisual or vibrissotactile cues, whereas olfactory-cued tasks have, to the best of our knowledge, been overlooked. Because we and others had detected widespread PrP^C expression throughout the olfactory system[9,10], we reasoned that olfactory-mediated behaviors might be affected in *Prnp*$^{-/-}$ mice.

The sense of smell is critical to the survival of many animals, mediating essential behaviors such as feeding and mating. The basic circuit of the olfactory system in mice and other mammals, from sensory epithelium to cortex, consists of only two projection synapses (peripheral sensory neuron to mitral cell in the olfactory bulb and mitral cell to pyramidal cell in the cortex) and two layers of inhibitory lateral processing (periglomerular and granule cells) in the olfactory bulb. In particular, mitral and granule cells make a unique dendrodendritic synapse in which mitral cells excite granule cells that reciprocally inhibit the mitral cell. This inhibitory circuit is thought to be involved in synchronizing mitral cell firing and enabling lateral inhibition[11,12].

Here we uncovered a previously unknown phenotype of *Prnp*$^{-/-}$ mice in the olfactory system by using a combination of genetic, behavioral and physiological techniques in a systems approach. We employed the so-called 'cookie-finding task', a test of broad olfactory acuity, to analyze a battery of mice, including PrP^C knockouts on multiple genetic backgrounds and transgenic mice in which *Prnp* expression was driven by cell type–specific promoters. In this test, PrP-deficient mice showed impaired behavior that was rescued in transgenic mice expressing PrP^C specifically in neurons but not in mice expressing only extra-neuronal PrP^C. *Prnp*$^{-/-}$ mice had altered behavior in an additional olfactory test (habituation-dishabituation), which was also rescued by transgenic neuronal PrP expression, suggesting the phenotype was olfactory specific.

With this evidence that the underlying alteration resided beyond the periphery, we investigated the odor-evoked electrophysiological properties of the olfactory bulb of PrP knockouts. In these mice, we detected alterations in the patterns of oscillatory activity in the olfactory bulb and in the plasticity of dendrodendritic synaptic transmission between granule cells and mitral cells. We propose that electrophysiological

[1]Department of Biological Sciences, Columbia University, 1212 Amsterdam Avenue, New York, New York 10027, USA. [2]Institute of Neuropathology, University Hospital Zürich, Schmelzbergstrasse 12, 8091 Zürich, Switzerland. [3]Present addresses: Ludwig Institute for Cancer Research, University of California at San Diego, 9500 Gilman Drive, La Jolla, California 92093, USA (M.P.) and Weill Medical College of Cornell University, 785 Mamaroneck Avenue, White Plains, New York 10605, USA (B.T.S.). Correspondence should be addressed to S.F. (sjf24@columbia.edu).

Received 24 July; accepted 6 November; published online 21 December 2008; doi:10.1038/nn.2238

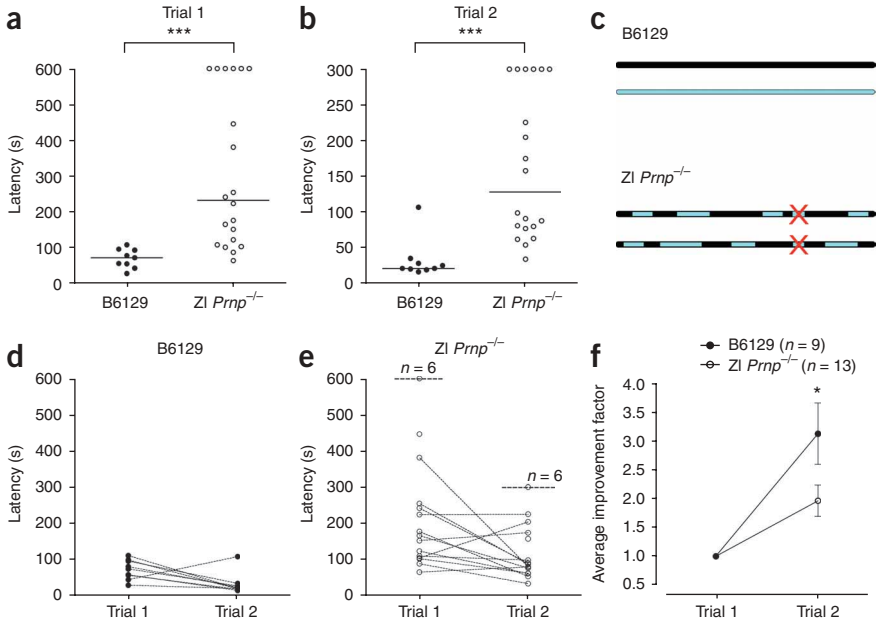

Figure 1 Impaired behavior of Zürich I *Prnp*$^{-/-}$ mice in the cookie-finding test. (**a**) Trial 1 of the cookie-finding test for B6129 (filled dots) and Zürich I line (ZI) *Prnp*$^{-/-}$ (open dots) mice. Each dot represents a single individual. Individuals that failed the trial were assigned the conservative score of 600 s, which corresponded to the total test time. Black lines represent medians. (**b**) Trial 2. Note that trial times were reduced to 5 min. Individuals that failed trial 2 were given the conservative score of 300 s. (**c**) Schematic diagram of the genetic makeup of the B6129 wild-type and Zürich I line *Prnp*$^{-/-}$ mice on a mixed B6 and 129 background. The red cross represents the knockout allele of *Prnp*. The black and cyan sections represent alleles of B6 and 129 origin, respectively. (**d**) Individual progression of each B6129 mouse from trial 1 to trial 2. (**e**) Individual progression from trial 1 to trial 2 of each Zürich I line *Prnp*$^{-/-}$ mouse, excluding animals that failed trial 1 or that found the cookie in trial 1 with a latency greater than 300 s and also failed trial 2. *n* is indicated for points that overlap exactly. (**f**) Average degree of improvement for wild-type (filled dots) and knockout (open dots) mice, calculated as $\sum$(T1/T2)/n, excluding animals that failed to find the cookie in trial 1 or that found the cookie in trial 1 with a latency greater than 300 s and also failed trial 2. Error bars represent ± s.e.m. * $P < 0.05$ (one-tailed unpaired *t* test), *** $P < 0.001$ (two-tailed Mann-Whitney test).

alterations at the dendrodendritic synapse in the olfactory bulb could underlie the behavioral phenotype that we found.

RESULTS

Prnp$^{-/-}$ mice show altered behavior in an olfactory task

We used a test that measures olfactory detection (cookie-finding test; **Fig. 1**)[13]. Mice that are faster at retrieving the cookie are thought to have a better sense of smell. The first of two successive trials reflected naive olfactory-mediated finding and the second indicated the mouse's ability to improve on the basis of positive reinforcement received in the first trial.

In trial 1, wild-type mice retrieved the cookie in a median latency time of 73 s, whereas *Prnp*$^{-/-}$ mice (Zürich I line; **Fig. 1c**) were significantly slower at 233 s ($P < 0.001$, Mann-Whitney test; **Fig. 1a**). Furthermore, close to a third of the *Prnp*$^{-/-}$ mice (6 out of 20) failed to find the cookie in the 10-min test time, whereas no wild-type mouse failed the test.

In trial 2, *Prnp*$^{-/-}$ mice were again significantly slower than wild types at retrieving the cookie (wild-type median, 20 s; *Prnp*$^{-/-}$ median, 127.5 s; $P < 0.001$, Mann-Whitney test; **Fig. 1b**). Even if those *Prnp*$^{-/-}$ mice that had failed Trial 1 were excluded from the analysis on the basis of their failure to have received positive reinforcement, the differences were still significant (wild-type median, 20 s; *Prnp*$^{-/-}$ median, 83.5 s; $P < 0.01$ Mann-Whitney test).

The slower latencies of *Prnp*$^{-/-}$ mice in both trials were not a result of a lack of exploration (as assessed by the number of crossings from one cage quadrant to another), a lack of appetite (as these mice readily consumed the cookie on finding it) or a metabolic alteration (all tested mice showed similar weight and daily food consumption regardless of genotype) (**Supplementary Fig. 1** online and data not shown). Furthermore, the difference between *Prnp*$^{-/-}$ and wild-type mice did not result from a locomotor deficiency in the knockouts, as both performed similarly in a control version of this experiment in which the cookie was presented on the surface of the bedding instead of being buried underneath it (**Supplementary Fig. 1**).

Comparing trials 1 and 2, we observed that wild-type mice improved from a median of 73 s to 20 s, whereas *Prnp*$^{-/-}$ mice improved, at best, from 233 s to 83.5 s. Eight out of nine wild-type mice improved between trials 1 and 2 (**Fig. 1d**), compared with only 8 out of 13 knockouts (and excluding those that had failed trial 1 or 2; **Fig. 1e**). We calculated an improvement factor corresponding to the average ratio of the latency in trial 1 versus trial 2. Overall, wild-type mice improved threefold (3.12 ± 0.53 s.e.m.), whereas *Prnp*$^{-/-}$ mice only improved twofold (1.97 ± 0.29; $P < 0.05$, one-tailed *t* test). The difference in the degree of improvement was even greater considering the floor effect on wild-type latencies resulting from the initial rapidity in trial 1. Thus, *Prnp*$^{-/-}$ mice showed impaired behavior in this odor-guided task.

Prnp$^{-/-}$ mouse behavior resembles that of anosmic mice

For comparison with a negative extreme of possible behaviors in this task, we tested a known anosmic mouse, the adenylyl cyclase type 3 (AC3) knockout (*Adcy3*$^{-/-}$). AC3 is a component of the olfactory transduction cascade that is necessary for generating action potentials in response to odorant binding at an odorant receptor. *Adcy3*$^{-/-}$ mice have been shown to be largely anosmic[14], although they retain residual olfactory capacity via their vomeronasal organ[15].

To control for the mixed genetic background of both the *Prnp*$^{-/-}$ and *Adcy3*$^{-/-}$ mice, we also tested both pure parental strains C57BL/6J (B6) and 129/SvEv (129). Because of animal availability, this experiment was conducted in a different facility, necessitating the retesting of the wild-type B6129 and Zürich I line *Prnp*$^{-/-}$ mice for comparison with our previous results. The altered environmental conditions may explain the raw data differences for the B6129 and *Prnp*$^{-/-}$ mice between the two experiments (**Fig. 2** versus **Fig. 1**).

Despite these differences, the same trend was apparent under both experimental conditions. All wild-type mice, regardless of strain, achieved much faster latencies to retrieve the cookie than either the *Prnp*$^{-/-}$ or *Adcy3*$^{-/-}$ mice, a substantial proportion of which failed both trials (**Fig. 2a**,**b**). In trial 1, *Prnp*$^{-/-}$ mice, similar to *Adcy3*$^{-/-}$ mice, trended toward slower latencies than wild types (wild-type medians:

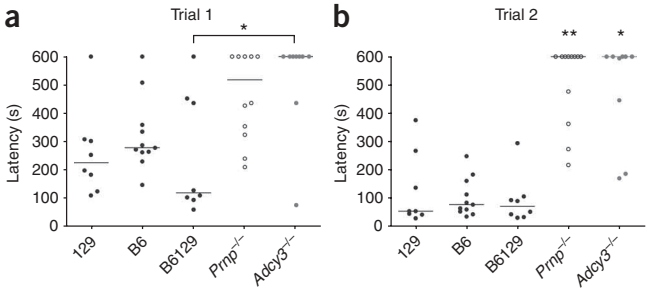

Figure 2 Zürich I *Prnp*$^{-/-}$ mouse behavior resembles that of a known anosmic mouse (*Adcy3*$^{-/-}$). (**a**) Scatter plot showing performance of wild-type strains 129, B6 and B6129 (black dots), Zürich I line *Prnp*$^{-/-}$ (open), and *Adcy3*$^{-/-}$ (gray) in trial 1 of the cookie-finding test. Individuals that failed to find the cookie in the test time were assigned the conservative score of 600 s, corresponding to the total test time. Black lines represent median values. (**b**) Trial 2 performances for the same mice. * $P < 0.05$, ** $P < 0.01$, Dunn's multiple comparison test. Note that values for B6129 wild-type and Zürich I line *Prnp*$^{-/-}$ mice differ from those in **Figure 1** because this test was performed under alternate experimental conditions.

225.5 s (129), 278 s (B6) and 119 s (B6129); *Prnp*$^{-/-}$ median, 518 s; *Adcy3*$^{-/-}$ median, 600 s; **Fig. 2a**). In trial 2, *Prnp*$^{-/-}$ mice continued to resemble *Adcy3*$^{-/-}$ mice, failing to improve and contrasting significantly with wild types (wild-type medians: 56 s (129), 79 s (B6) and 73 s (B6129 F1); *Prnp*$^{-/-}$ and *Adcy3*$^{-/-}$ mice, both 600 s, $P < 0.01$ and $P < 0.05$, respectively, Dunn's multiple comparison test; **Fig. 2b**).

Prnp$^{-/-}$ phenotype extends to other genetic backgrounds

Because the phenotypic impairment had been detected in a *Prnp*$^{-/-}$ mouse on mixed genetic background and lacking wild-type littermates, it is possible that the phenotype that we detected was the result of a genetic factor other than the absence of PrP^{C}. We thus tested two additional *Prnp*$^{-/-}$ lines (**Fig. 3**), one congenic with B6 (Nagasaki; **Fig. 3c**) and one isogenic with 129 (Edinburgh; **Fig. 3i**), reasoning that if the phenotype were also observable on these backgrounds, it might indeed be attributable to PrP deficiency rather than to another genetic factor.

The Nagasaki *Prnp*$^{-/-}$ mouse line is not usually a line of choice for phenotypic analysis of PrP deficiency, as the mice develop late-onset ataxia as a result of spurious upregulation of the downstream gene *Prnd*[16]. However, these mice show no symptoms before 1 year of age, and we tested them at the presymptomatic age of 7–10 weeks, which is well before their decline (70 weeks).

We noticed an effect of a predominantly B6 genetic background on cookie-finding behavior; Nagasaki *Prnp*$^{-/-}$ mice scored faster latencies than the Zürich I line (Nagasaki median, 155 s; Zürich I line median, 223s). In trial 1, not a single Nagasaki *Prnp*$^{-/-}$ mouse failed to find the cookie, whereas 6 out of 20 Zürich I line *Prnp*$^{-/-}$ mice failed (**Fig. 3a** versus **Fig. 1a**). Nevertheless, the Nagasaki knockouts were significantly slower than their wild-type counterparts (wild-type median, 76.5 s; *Prnp*$^{-/-}$, median 155 s; $P < 0.05$, Mann-Whitney test; **Fig. 3a**), thus revealing a phenotype similar to the one that we detected in the Zürich I *Prnp*$^{-/-}$ line.

In trial 2, Nagasaki knockouts were significantly slower than their wild-type counterparts (wild-type median, 27.5 s; *Prnp*$^{-/-}$ median, 89.5 s; $P < 0.001$, Mann-Whitney test; **Fig. 3b**). The fastest knockout latencies in trial 2 clustered around 62 s, close to double the median wild-type latency (**Fig. 3b**). Although the knockouts tended to improve in trial 2 (**Fig. 3e**), they failed to improve as much as wild types (**Fig. 3d**). Overall, the *Prnp*$^{-/-}$ mouse improvement was almost twofold less than wild types (wild-type improvement factor, 3.84 ± 0.68 s.e.m.; *Prnp*$^{-/-}$ improvement factor, 1.96 ± 0.32; $P < 0.05$, one-tailed unpaired *t* test; **Fig. 3f**). The phenotype exhibited by Zürich I line *Prnp* knockouts was thus confirmed by another knockout line.

However, because of residual 129 alleles that are tightly linked to the knockout allele in the Nagasaki *Prnp*$^{-/-}$ mouse line, which is otherwise congenic with B6, we still could not fully attribute the phenotype to the absence of PrP. We thus tested a third *Prnp*$^{-/-}$ mouse line, the

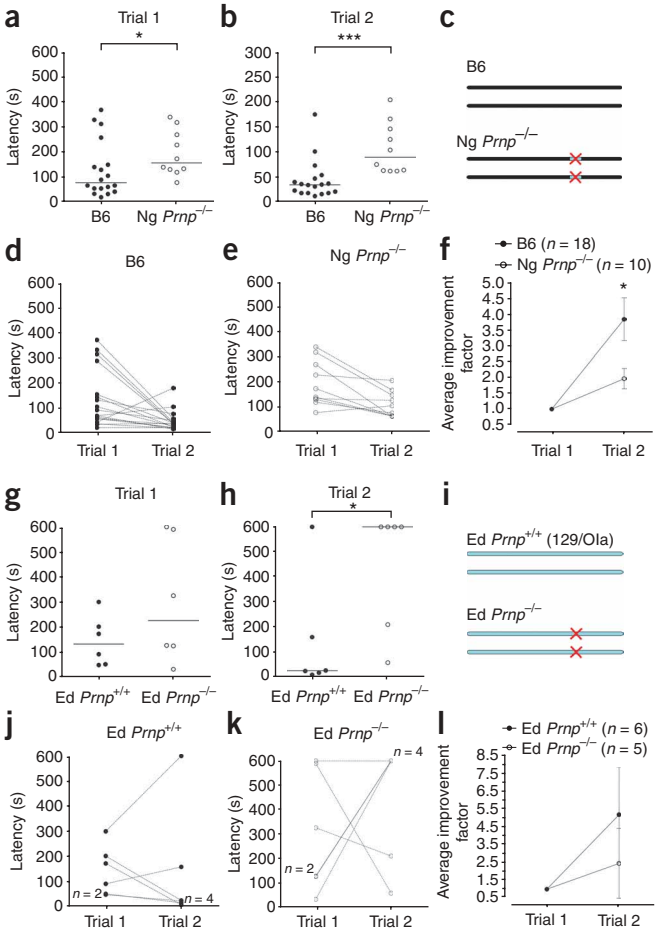

Figure 3 The cookie-finding phenotype is manifest in *Prnp* knockouts on other genetic backgrounds. (**a**) Trial 1 of the cookie-finding test for B6 (filled) and Nagasaki (Ng) *Prnp*$^{-/-}$ (open). (**b**) Trial 2 for mice shown in **a**. Note the reduced timescale of 5 min. (**c**) Schematic diagram of genetic background of the B6 wild-type and congenic Nagasaki *Prnp*$^{-/-}$ mice. Black and cyan sections represent alleles of B6 and 129 origin, respectively. The red cross represents the knockout allele. (**d**) Individual progression from trial 1 to trial 2 of each B6 mouse. (**e**) Individual progression from trial 1 to trial 2 of each Nagasaki *Prnp*$^{-/-}$ mouse. (**f**) Average degree of improvement for B6 (filled) and Nagasaki *Prnp*$^{-/-}$ (open). Error bars ± s.e.m. (**g**) Trial 1 of the cookie-finding test for Edinburgh (Ed) *Prnp*$^{+/+}$ (filled) and Edinburgh *Prnp*$^{-/-}$ (open) mice. (**h**) Trial 2 for mice shown in **g**. (**i**) Schematic diagram of genetic background of the Edinburgh *Prnp*$^{-/-}$ and isogenic wild-type littermates (129/Ola background). Cyan sections represent alleles of 129/Ola origin. The red cross represents the knockout allele. (**j**) Individual progression from trial 1 to trial 2 of each 129/Ola wild-type mouse. (**k**) Individual progression from trial 1 to trial 2 of each Edinburgh *Prnp*$^{-/-}$ mouse. (**l**) Average degrees of improvement for Edinburgh *Prnp*$^{-/-}$ (open) and *Prnp*$^{+/+}$ littermates (filled) were not significantly different because of the low *n*. Error bars ± s.e.m. Black lines represent median values. * $P < 0.05$ (one-tailed unpaired *t* test), *** $P < 0.001$ (two-tailed Mann Whitney test).

Table 1 Mouse strains tested for cookie finding behavior

Strain name	Abbreviation	Type	Description	Reference number	Genetic background	PrP^C expression
C57BL/6J × 129/Sv F1 hybrid	B6129	Wild type	Wild-type hybrid	Methods	50% C57BL/6J, 50% 129S/Sv	Wild type
Zürich I *Prnp*$^{-/-}$		Knockout	*Prnp* knockout	1	C57BL/6J × 129/Sv mixed background	None
Nagasaki *Prnp*$^{-/-}$		Knockout	*Prnp* knockout with late-onset ataxia as a result of upregulation of *Prnd*	42	Congenic C57BL/6J	None
Edinburgh *Prnp*$^{-/-}$		Knockout	*Prnp* knockout	38	Isogenic 129/Ola	None
Tg20	Tg20	Transgenic	*Prnp* driven by endogenous *Prnp* promoter ('half-genomic construct')	43	Zürich I *Prnp*$^{-/-}$ background	Overexpression in wild-type locations
NSE-PrP	NSE-PrP	Transgenic	*Prnp* driven by *Eno2* promoter	44	Zürich I *Prnp*$^{-/-}$ background	Neurons only (central and peripheral nervous system)
MBP-PrP	MBP-PrP	Transgenic	*Prnp* driven by *Mbp* promoter	45	Zürich I *Prnp*$^{-/-}$ background	Oligodendrocytes and Schwann cells only
Tg306	CD19-PrP	Transgenic	*Prnp* driven by *CD19* promoter	46	Zürich I *Prnp*$^{-/-}$ background	B cells only
Tg33	Lck-PrP	Transgenic	*Prnp* driven by *Lck* promoter	47	Zürich I *Prnp*$^{-/-}$ background	T cells and some neurons
Prn knockout	*Prn*$^{-/-}$	Knockout	Double knockout of *Prnp* and homologous downstream gene *Prnd*	48	C57BL/6J × 129/Sv mixed background	None

All knockout and transgenic animals presented in this table are on the Zürich I mixed B6 and 129 genetic background. Notably, the transgenic lines were generated by microinjection of *Prnp* transgenes into homozygous Zürich I *Prnp*$^{-/-}$ zygotes, thus enabling direct comparisons between the different lines.

Edinburgh line, on a pure 129/Ola background. These mice are isogenic with their wild-type counterparts, thus circumventing the problem of mixed background (**Fig. 3i**).

On this background too the phenotype was apparent. Although *Prnp*$^{+/+}$ mice only trended toward faster latencies in trial 1 (wild-type median, 133.5 s; *Prnp*$^{-/-}$ median, 227 s; **Fig. 3g**), they were significantly faster in trial 2 (wild-type median, 26 s; *Prnp*$^{-/-}$ median, 600 s; $P < 0.05$, Mann-Whitney test; **Fig. 3h**). In trial 2, four out of six wild-type mice improved to very fast latencies (**Fig. 3j**), whereas *Prnp*$^{-/-}$ mice showed no clear trend toward improvement, with four out of six failing the trial (**Fig. 3k**). The average improvement factors were not significantly different as a result of the small sample size (wild type, 5.16 ± 2.7; *Prnp*$^{-/-}$, 2.44 ± 2.0; **Fig. 3l**).

Thus, although the severity of the phenotype varied with the genetic background, we found that *Prnp*$^{-/-}$ mice showed impaired behavior in the cookie-finding test on a mixed B6 × 129, a congenic B6 and an isogenic 129/Ola background.

The *Prnp*$^{-/-}$ phenotype is rescued by neuronal PrP expression

We next asked whether neuronal-specific PrP^C expression could selectively rescue the phenotype. We tested a battery of knockout and transgenic mice that were all on the Zürich I mixed background (**Table 1** and **Fig. 4**). We pooled animals according to whether or not they expressed *Prnp* in neurons, which we confirmed by *in situ* hybridization, and examined whether neuronal PrP^C improved cookie-finding performance. The difference between the two groups was notable. In both trials, the mice lacking neuronal PrP^C were twice as slow as mice that expressed PrP^C in neurons ($P < 0.001$, Mann-Whitney test; **Fig. 4a**,**b**).

This difference was not a result of the effect of any particular strain, as shown by separating the groups into individual datasets (**Fig. 4c**,**d**). Overexpression of PrP^C on a *Prnp*$^{-/-}$ background (Tg20 mouse line) exerted a rescuing effect, as did NSE-driven expression of PrP^C (that is, neuronal-specific expression, NSE-PrP mouse line). Both these lines closely resembled the B6129 wild types (**Fig. 4c**,**d**) with trial 1 medians all being below 100 s and trial 2 medians being below 40 s. In contrast, when PrP was expressed in non-neuronal cells such as myelinating glia (MBP-PrP mouse line) or B cells (CD19-PrP mouse line), the mice were not rescued and phenotypically resembled the Zürich I line *Prnp*$^{-/-}$ mice (**Fig. 4c**,**d**). In addition, *Prnp* and *Prnd* (a downstream gene of *Prnp*) double-knockout mice (*Prn*$^{-/-}$) were also impaired. All mice lacking neuronal PrP^C showed median latencies above 160 s in trial 1 (**Fig. 4c**) and above 125 s in trial 2 (**Fig. 4d**). The case of the Lck-PrP mouse line (**Fig. 4c**,**d**) will be discussed below.

Lck-PrP mice express neuronal *Prnp* in the olfactory bulb

Notably, the Lck-PrP transgenic line (**Fig. 4c**,**d**) appeared to be at least partially rescued by its particular pattern of PrP expression. *Lck* encodes lymphocyte protein tyrosine kinase and is highly expressed in T cells. By *in situ* hybridization, however, we found that the *Lck* promoter drove *Prnp* expression in several brain areas (**Fig. 5**), including the olfactory bulb (in juxtaglomerular cells, mitral/tufted cells and granule cells; **Fig. 5a**) and the cerebellum (**Fig. 5b**). In contrast, CD19-PrP mice (B cell–specific expressers) showed no such staining (**Fig. 5d**). Other reports have also detected an active *Lck* promoter in neurons of the brain, including in olfactory areas[17] (Allen Brain Atlas, http://www.brain-map.org/).

We excluded the Lck-PrP line from the groups listed above (**Fig. 4a**,**b**), as PrP^C was expressed in some, but not all, neurons in these mice. However, the substantial rescue mediated by the particular pattern of PrP expression in Lck-PrP mice could, in fact, point to neurobehavioral regions of importance. In particular, PrP^C was not expressed in the olfactory epithelium of these mice (**Fig. 5c**), suggesting that the basis for the impairment was not peripheral. In addition, we observed normal odor-evoked electro-olfactogram responses from *Prnp*$^{-/-}$ olfactory epithelium (**Supplementary Fig. 2** online). The physiological correlates underlying the impaired behavior thus appeared to reside in central structures. To streamline our investigation, we restricted our subsequent experiments to the use of the B6129 wild type, the Zürich I *Prnp*$^{-/-}$ line and the NSE-PrP transgenic line (**Fig. 4e–f**).

Altered behavior of *Prnp*$^{-/-}$ mice in another olfactory task

To help ascertain whether the phenotype of the *Prnp*$^{-/-}$ mice in the cookie-finding test was indeed olfactory specific, we carried out an

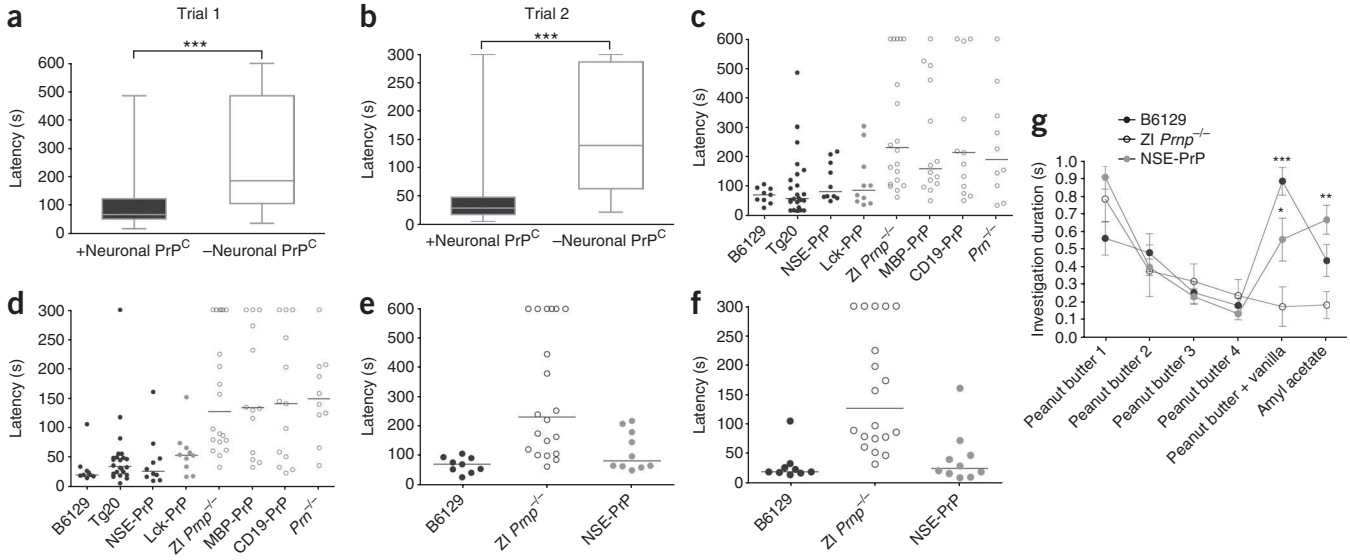

Figure 4 Neuronal PrP expression rescues the cookie-finding phenotype. (**a**). Trial 1 for all lines, neuronal PrP^C expressers (+Neuronal PrP^C: B6129, Tg20 and NSE-PrP; filled) and neuronal PrP^C-deficient mice (–Neuronal PrP^C: Zürich I *Prnp*$^{-/-}$, MBP-PrP, CD19-PrP and *Prnp*$^{-/-}$; open). For +Neuronal PrP^C: minimum = 19 s, lower quartile = 53 s, median = 70.5 s, upper quartile = 133 s, maximum = 569 s. For –Neuronal PrP^C: minimum = 37 s, lower quartile = 106.5 s, median = 187 s, upper quartile = 485.5 s, max = 600 s. (**b**) Trial 2. Note reduced timescale of 5 min. For +Neuronal PrP^C: minimum = 6 s, lower quartile = 19.5 s, median = 30 s, upper quartile = 49 s, maximum = 300 s. For –Neuronal PrP^C: min = 23 s, lower quartile = 64 s, median = 140 s, upper quartile = 286.5 s, max = 300 s. Individuals that failed the trial were given the conservative score of the total trial length. *** $P < 0.001$, two-tailed Mann-Whitney test. (**c**,**d**) Breakdown by strain of data in **a** and **b**, respectively. Filled dots represent strains expressing PrP^C in neurons and open dots represent those that do not. Because it expressed PrP^C only in some neurons, Lck-PrP (gray) was not included in either group in **a** and **b**. Lines represent medians. (**e**,**f**) Results for the B6129, Zürich I line *Prnp*$^{-/-}$ and NSE-PrP mouse lines, our three representative strains. (**g**) Altered phenotype of Zürich I line *Prnp*$^{-/-}$ mice in the habituation-dishabituation test. All mice habituated to the first odor (peanut butter). B6129 (black) and NSE-PrP (gray) mice showed strong renewed interest in the novel odors (peanut butter + vanilla mix and amyl acetate), whereas Zürich I line *Prnp*$^{-/-}$ mice (open dots) failed to respond to them. Error bars ± s.e.m. * $P < 0.05$, ** $P < 0.01$, ***$P < 0.001$, two-way ANOVA, Bonferroni post test.

additional olfactory behavior test, the habituation-dishabituation assay[18]. In this test, successive presentations of the same stimulus odor result in a decrease of investigatory behavior (habituation). An increase in the mouse's interest when a novel odor is presented (dishabituation) is interpreted as an ability to discriminate the difference between the two odorants. We used a peanut butter odor as the habituation odor, a mixture of peanut butter and vanilla as the first novel odor and amyl acetate as a second novel odor.

Zürich I line *Prnp*$^{-/-}$ mice habituated to the first odor similar to controls (B6129 and NSE-PrP). However, although the controls showed increased interest in the novel odors, *Prnp*$^{-/-}$ mice did not, indicating altered olfactory behavior (**Fig. 4g**). Together with the results of the cookie-finding test, this result strongly suggests that the phenotype was indeed olfactory specific.

Altered responses to odor input in *Prnp*$^{-/-}$ olfactory bulb

We focused on the electrophysiological properties of the olfactory bulb circuitry because the olfactory bulb is the first brain area to process olfactory information and the behaviorally rescued Lck-PrP mice expressed PrP^C in neurons of the olfactory bulb. We recorded local field potentials (LFPs, **Fig. 6**) from this area because they reflect the average current flow from synaptic and spiking activity around the

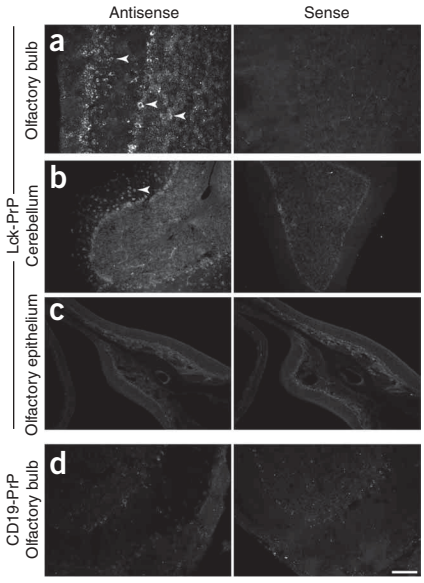

Figure 5 Lck-PrP transgenic mice express some neuronal PrP^C. (**a**–**d**) Fluorescent *in situ* hybridization for detection of *Prnp* transcripts in the olfactory bulb and cerebellum of transgenic Lck-PrP mice (**a**–**c**) and CD19-PrP mice (**d**). Left, signal from antisense *Prnp* probe. Right, negative control sense probes. The *Prnp* probe used here was such that it only recognized wild-type *Prnp* transcripts and not the truncated *Prnp* transcript that is produced from the Zürich I *Prnp* knockout allele. All slides were detected over an equal amount of time. *Prnp* was expressed in cells of the olfactory bulb in Lck-PrP mice (**a**). From left to right, arrows point to examples of a *Prnp*-positive cell in the external plexiform layer, a mitral cell and granule cells. *Prnp* expression in the cerebellum of Lck-PrP mice (**b**). Arrow points to an example of a *Prnp*-positive cell in the molecular layer. Some Purkinje cells and granule cells are also labeled. Lck-PrP mice do not express *Prnp* in the olfactory epithelium (**c**). *Prnp* was not expressed in the olfactory bulb of CD19-PrP mice (**d**). The low signal that can be observed is a result of the background staining. Scale bar represents 100 μm.

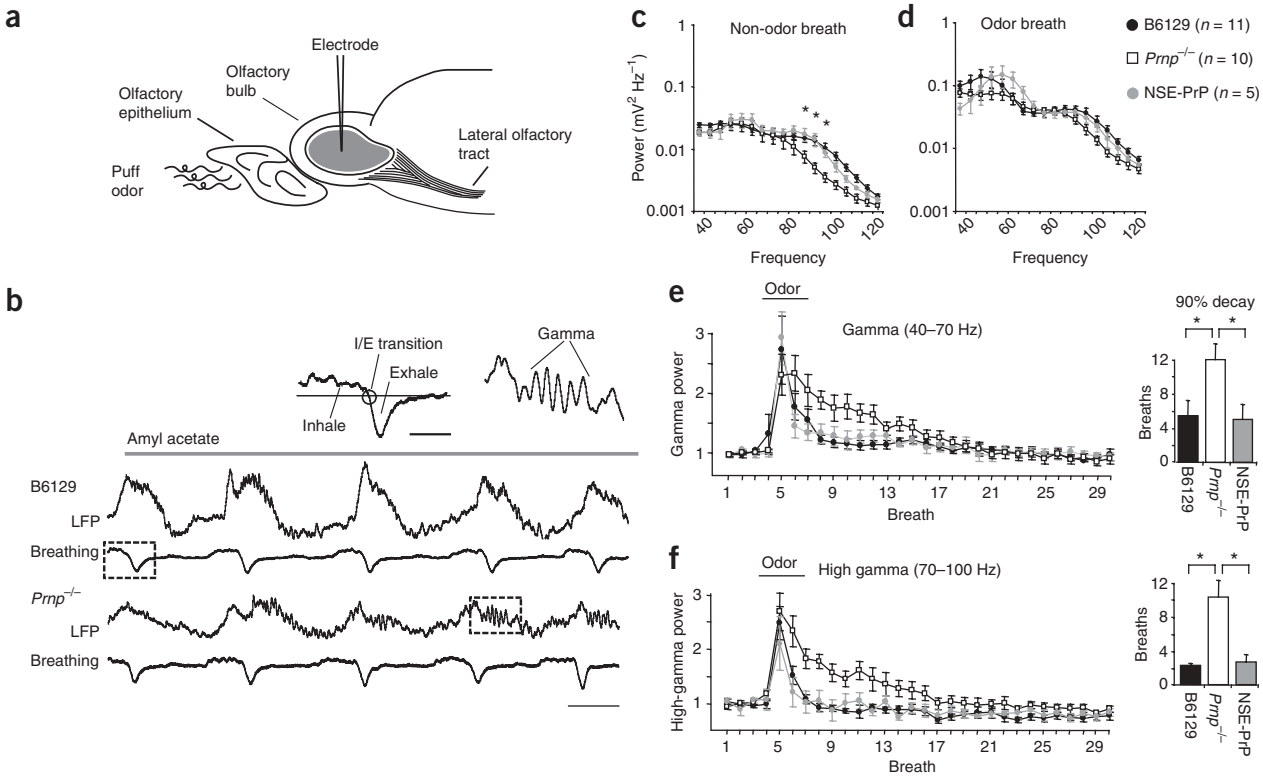

Figure 6 Power of LFPs and duration of the odor response in *Prnp*$^{-/-}$ mice. (**a**) LFPs were measured *in vivo* from the granule cell layer in the main olfactory bulb of anesthetized mice. (**b**) Example LFP traces from a B6129 mouse (top) and a *Prnp*$^{-/-}$ mouse (bottom) with corresponding breathing traces. Odor presentation was triggered by the first inhalation/exhalation transition (I/E, circle in left inset), but the odor was not detected until the following inhalation. Right inset, example of gamma-range oscillations. (**c**) Average power spectra of a non-odor breath from wild-type (B6129, $n = 11$), PrP knockout (*Prnp*$^{-/-}$, $n = 10$) and neuronal PrP–expressing transgenic (NSE-PrP, $n = 5$) mice. The power of high-gamma oscillations was significantly lower in PrP knockouts compared with both control strains. (**d**) In an odor-containing breath, the power of all frequencies increased in all groups. (**e**) The power of gamma oscillations in each breath is plotted as fold change from baseline for 30 breaths around a 2-s pulse of amyl acetate. *Prnp*$^{-/-}$ mice had an extended oscillatory response to odor in the gamma frequency band, as indicated by the time (in number of breaths) for the response to decay to 90% of its peak. (**f**) High-gamma oscillations in the PrP knockout also showed a significantly longer decay compared with both control strains. * $P < 0.05$ using one-way ANOVA with *post hoc* PLSD. Scale bars represent 200 ms in **b** and 50 ms in inset.

recording site (**Fig. 6a**). Furthermore, as various frequencies of LFP oscillations specifically reflect different processes, an LFP signal simultaneously assays different types of physiological events. For example, gamma oscillations in anesthetized mice (40–100 Hz) reflect activity originating from a specific synapse between output neurons (mitral cells) and interneurons (granule cells) called the dendrodendritic synapse[19,20].

In the olfactory bulb of anesthetized mice, LFP oscillations are coupled to the breathing cycle, allowing us to use breaths as a measure of time (**Fig. 6b**). We measured the power of LFP oscillations at frequencies ranging from 2–120 Hz over a sequence of breaths surrounding odor stimulation. We did not find alterations at beta (10–40 Hz) and delta frequencies (breathing rate, 2–3 Hz; data not shown), and so we focused our analysis on gamma (40–70 Hz) and high-gamma (70–100 Hz) oscillations.

During normal (odorless) respiration, *Prnp*$^{-/-}$ animals showed significantly lower power than B6129 and NSE-PrP control mice at 88 Hz (mean power in 10^{-3} mV^2 Hz^{-1}; *Prnp*$^{-/-}$, 9.01 ± 2.11; B6129, 18.80 ± 2.96; NSE-PrP, 22.1 ± 5.57; ANOVA, $P < 0.05$; **Fig. 6c**), 93 Hz (*Prnp*$^{-/-}$, 5.81 ± 1.17; B6129, 17.0 ± 3.05; NSE-PrP, 18.0 ± 4.56; ANOVA, $P < 0.05$) and 98 Hz (*Prnp*$^{-/-}$, 3.99 ± 0.73; B6129, 12.80 ± 2.32; NSE-PrP, 10.50 ± 1.92; ANOVA, $P < 0.05$). Similar analysis of the first breath of odor showed an increase in the power of oscillations in gamma and high-gamma compared with odorless respiration but without any significant differences between the groups (**Fig. 6d**). Analysis with finer temporal resolution was necessary to resolve any differences (**Fig. 7**).

Plotting the average band power for every breath allowed us to observe changes in the kinetics of the odor response. Odor stimulation elicited a strong response in both gamma (**Fig. 6e**) and high-gamma (**Fig. 6f**) bands, visible as a sharp increase in power followed by a slow decay. In *Prnp*$^{-/-}$mice, this decay occurred over a significantly larger number of breaths than in the control group for both gamma-band oscillations (decay time in mean number of breaths: *Prnp*$^{-/-}$, 12.0 ± 1.8; B6129, 5.5 ± 1.8; NSE-PrP, 5.0 ± 1.7; ANOVA, $P < 0.05$; **Fig. 6e**) and high-gamma oscillations (*Prnp*$^{-/-}$, 10.0 ± 1.9; B6129, 2.2 ± 0.3; NSE-PrP, 2.6 ± 0.8; ANOVA, $P < 0.001$; **Fig. 6f**). Together, the lower power and sustained duration of high-frequency oscillations in the *Prnp*$^{-/-}$ mice suggested that the temporal structure of oscillations in a single breath might also be altered.

LFP oscillations poorly timed to breathing in *Prnp*$^{-/-}$ mice

To better understand the oscillatory phenotype, we further analyzed our LFP data to measure the emergence and extinction of LFP oscillations in a breathing cycle. Gamma oscillations in the granule cell layer of the olfactory bulb emerged during exhalation and were

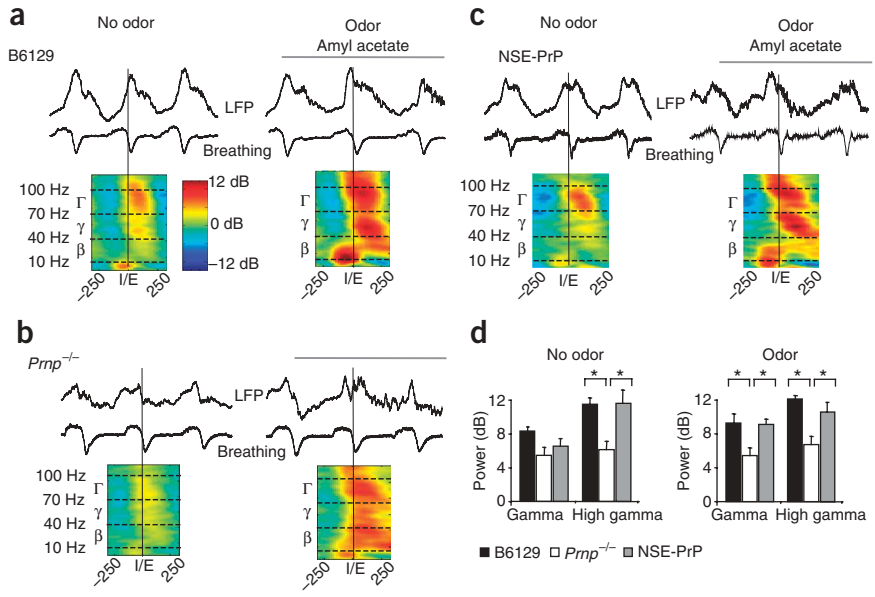

Figure 7 High-frequency oscillations in PrP knockouts are dampened in the course of a single breath. Example waveforms from single mice demonstrating how band power in high-gamma (Γ, 70–100 Hz), gamma (γ, 40–70 Hz) and beta (β, 10–40 Hz) frequencies changed around the point at which a mouse began to exhale (I/E transition, the midline of the spectrograms as marked by vertical lines, units in ms). The left example is a breath without odor stimulation and the right contains the first inhalation of an odor pulse. Below each LFP and breathing waveform is the averaged spectrogram from the entire group, corresponding to breath 1 and breath 5 (dashed boxes in **Supplementary Fig. 3**). (**a**–**c**) B6129, (**a**) *Prnp*$^{-/-}$ (**b**) and NSE-PrP (**c**) mice each showed similarly structured oscillatory patterns around a non-odor breath and an odor breath. (**d**) However, the difference between the band-averaged peak and subsequent trough of spectral power indicate that *Prnp*$^{-/-}$ mice have less change in the high-gamma band and less change during odor presentation in the gamma band. * $P < 0.05$ using one-way ANOVA with *post hoc* PLSD.

extinguished shortly after (**Fig. 7a–c**). To our surprise, the total range of oscillatory power during a breath was smaller in the *Prnp*$^{-/-}$ mice (**Fig. 7b**) compared with B6129 and NSE-PrP mice (**Fig. 7a,c**). Furthermore, the distribution of oscillatory power in the *Prnp*$^{-/-}$ mice was temporally diffuse across an odor breath (**Fig. 7b**), an alteration that was sustained in a series of breaths following odor exposure (**Supplementary Fig. 3** online).

We quantified the range of oscillatory power in a non-odor and an odor-containing breath (**Fig. 7** and **Supplementary Fig. 3**) by taking the difference between the peak of power and the following trough. In a non-odor breath, the change in power of high-gamma oscillations in the *Prnp*$^{-/-}$ mice was reduced compared with B6129 and NSE-PrP mice (mean change in power (dB): *Prnp*$^{-/-}$, 6.5 ± 0.9; B6129, 11.5 ± 0.8; NSE-PrP, 11.6 ± 1.5; **Fig. 7d**). Similarly, in an odor-containing breath, both gamma and high-gamma oscillations showed less change in power in *Prnp*$^{-/-}$ mice (*Prnp*$^{-/-}$, 5.9 ± 0.9; B6129, 9.7 ± 1.1; NSE-PrP, 9.5 ± 0.6; **Fig. 7d**).

Oscillations at these high-frequency bands (gamma and high gamma) are believed to result from activity at the dendrodendritic synapse[19,20]. The observed alterations in both power and timing suggested that the properties of the dendrodendritic synapse might be affected in the *Prnp*$^{-/-}$ mice.

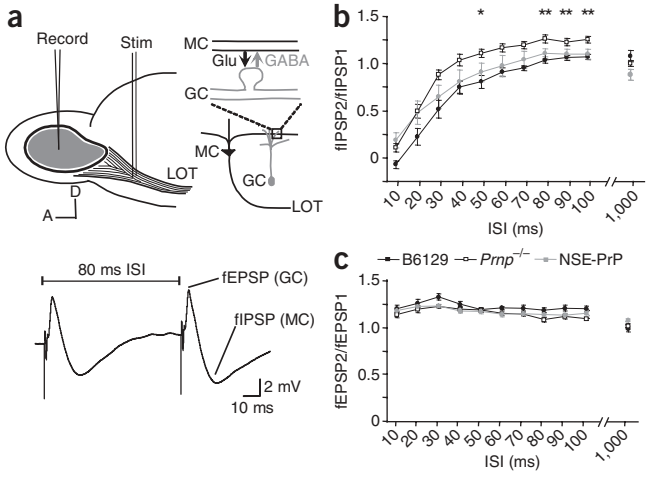

Figure 8 Paired-pulse synaptic plasticity of field potentials in the GCL after LOT stimulation. (**a**) Top, diagram illustrating the stimulation procedure. GC, granule cell; Glu, glutamate; LOT, lateral olfactory tract; MC, mitral cell. Middle, example trace following LOT paired-pulse stimulation (80 ms interstimulus interval, ISI). (**b**) Paired-pulse ratio of the evoked negative potential corresponding to mitral cell fIPSP. ** indicates significant differences between both control groups and *Prnp*$^{-/-}$ (one-way ANOVA, $P < 0.05$); * indicates significance from B6129 (one-way ANOVA with *post hoc* PLSD, $P < 0.05$). (**c**) Paired-pulse ratio of the evoked positive potential, corresponding to granule cell fEPSP for B6129 (filled black dots, $n = 7$), *Prnp*$^{-/-}$ (open dots, $n = 9$) and NSE-PrP (filled gray dots, $n = 10$) mice.

Altered paired-pulse plasticity of dendrodendritic synapse

We next examined the *Prnp*$^{-/-}$ dendrodendritic synapse for changes that could underlie the observed behavioral phenotypes. We focused on the short-term plasticity of this synapse, as our LFP results suggested that *Prnp*$^{-/-}$ mice might have disrupted synchronization between breathing and oscillations, perhaps reflecting altered facilitation or depression of this synapse. We therefore carried out paired-pulse stimulation of the synapse by antidromically exciting mitral cells from their axon bundle in the lateral olfactory tract (LOT) (**Fig. 8a**). This stimulation procedure produces distinct field potentials corresponding to granule cell excitation (field excitatory postsynaptic potentials, fEPSPs) followed by mitral cell inhibition[21,22] (field inhibitory postsynaptic potentials, fIPSPs; **Fig. 8a**).

In *Prnp*$^{-/-}$ mice, reciprocal inhibition of mitral cells (fIPSP) showed unusual facilitation over a range of interstimulus intervals (**Fig. 8b**). B6129 and NSE-PrP mice had a significantly facilitated paired-pulse ratio from the *Prnp*$^{-/-}$ mice at intervals between 80 and 100 ms, and B6129 mice also showed a significantly different ratio at 50 ms (ANOVA with Fisher's PLSD, $P < 0.05$). Notably, facilitation of the fIPSP in the *Prnp*$^{-/-}$ mice was not accompanied by any differences in the plasticity of the granule cell fEPSPs (**Fig. 8c**).

DISCUSSION

Here we describe a previously unknown olfactory behavioral phenotype of *Prnp*$^{-/-}$ mice and physiological alterations in their olfactory bulb. The cookie-finding phenotype was manifest in three *Prnp*$^{-/-}$ lines on alternate genetic backgrounds, which is strong evidence of its